

Indistinguishable single photons with flexible electronic triggering

Adetunmise C. Dada,^{1,*} Ted S. Santana,¹ Ralph N. E. Malein,¹ Antonios Koutroumanis,¹
Yong Ma,^{1,†} Joanna M. Zajac,¹ Ju Y. Lim,^{2,‡} Jin D. Song,² and Brian D. Gerardot¹

¹*Institute for Photonics and Quantum Sciences, SUPA,
Heriot-Watt University, Edinburgh EH14 4AS, United Kingdom*

²*Center for Opto-Electronic Convergence Systems,
Korea Institute of Science and Technology, Seoul, Korea*

A key ingredient for quantum photonic technologies is an on-demand source of indistinguishable single photons. State-of-the-art indistinguishable-single-photon sources typically employ resonant excitation pulses with fixed repetition rates, creating a string of single photons with predetermined arrival times. However, in future applications, an independent electronic signal from a larger quantum circuit or network will trigger the generation of an indistinguishable photon. Further, operating the photon source up to the limit imposed by its lifetime is desirable. Here we report on the application of a true on-demand approach in which we can electronically trigger the precise arrival time of a single photon as well as control the excitation pulse duration, based on resonance fluorescence from a single InAs/GaAs quantum dot. We investigate in detail the effect of finite duration of an excitation π pulse on the degree of photon antibunching. Finally, we demonstrate that highly indistinguishable single photons can be generated using this on-demand approach, enabling maximum flexibility for future applications.

I. INTRODUCTION

Single photons remain prime candidates for realising scalable schemes of quantum communication [1] and linear optical quantum computing [2, 3]. The performance of such schemes rely critically on the indistinguishability of the single photons [4], in particular for key applications such as quantum repeaters [5] and boson sampling [6, 7]. Of the various types of single photon sources [8, 9], semiconductor quantum dot (QD) systems are particularly promising for generating indistinguishable single photons because they offer a robust platform in which a single quantum system can be embedded within semiconductor devices and designed into bright single- and entangled-photon sources. The ideal single-photon source for quantum information processing (QIP) applications is one which generates a pure single photon Fock state *on demand*, i.e., in response to an independent trigger signal from a user. Pulsed resonance fluorescence (RF) has been identified as the optimal way to deterministically generate high-quality photons with minimal dephasing. However, good quality pulsed RF systems have so far utilised pulsed excitation generated by lasers with fixed repetition rates (~ 80 MHz) [10–15]. While this type of triggering could be said to be *deterministic*, it is not *on-demand* since a user in this case has limited control over the excitation pulse arrival time and duration.

Here, we apply a flexible scheme for pulsed RF which triggers the generation of highly indistinguishable single photons such that true on-demand operation is achieved via real-time electronic control. Our system uses a GHz-bandwidth electro-optic modulator (EOM) to modulate the output of a tunable continuous-wave (CW) laser for resonant excitation of a QD emitting at ~ 960 nm. In turn, the EOM is driven by a fast programmable electronic pulse-pattern generator (PPG). Such flexibility will greatly benefit practical applications of single photons in quantum technologies.

Key performance measures for an on-demand single photon source include: the efficiency, defined as the probability to detect a photon for a given electronic trigger; the purity, defined by the degree of antibunching as quantified by the second-order correlation function at zero delay; the degree of indistinguishability between individual photons as measured, e.g., by the Hong–Ou–Mandel (HOM)-type two-photon interference (TPI) visibility [16]; and crucially, the ability to determine or adjust, on demand, the timing and sequence of trigger pulses.

Considerable effort has been made towards realizing on-demand triggering of single photon generation by directly driving a QD electrically. GHz-bandwidth electrical pulses (with pulse width $w > 270$ ps) have been used to rapidly modulate the QD emission in resonant or non-resonant excitation [17–19]. Unfortunately the single photon purity in such hybrid schemes is less than ideal.

Similar effects have been observed when using an EOM to generate optical trigger pulses for a single-photon source (e.g., Ref. [20], $w = 500$ ps) where significant overlap between quantum dot RF pulses results in a quasi-CW stream of RF photons. EOM-generated op-

* a.c.dada@hw.ac.uk

† Current address: Chongqing Institute of Green and Intelligent Technology, Chinese Academy of Sciences, Chongqing, China 400714

‡ Current address: Korea Photonics Technology Institute, Gwangju 61007, Korea

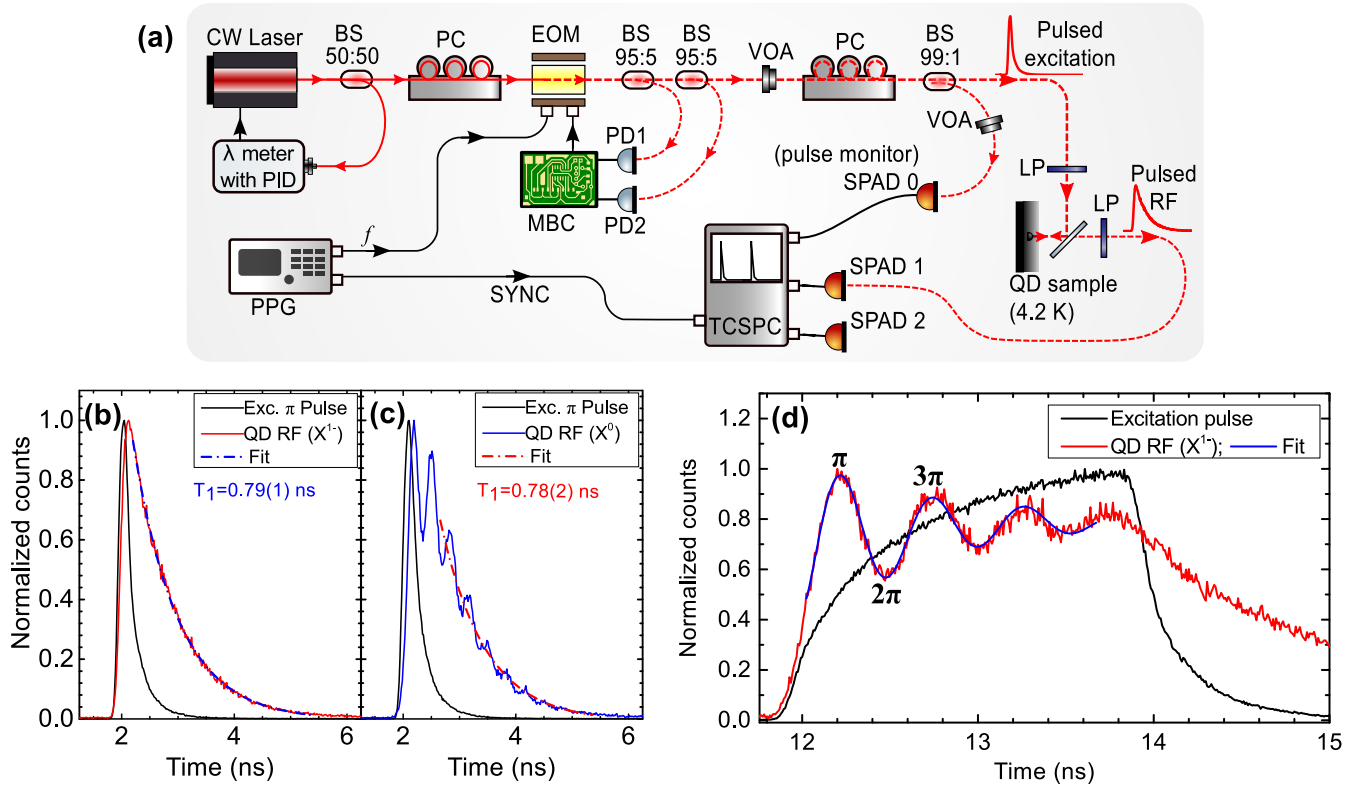


FIG. 1. (a) **Flexibly-triggered generation of resonance fluorescence from a quantum dot.** We modulate the CW laser output using a 20 Gb/s electro-optic modulator (EOM) driven by a pulse-pattern generator (PPG) capable of custom pulse patterns at up to a frequency of $f = 3.35$ GHz. A modulator bias controller (MBC) optoelectronic circuit maintains the high extinction ratio of the excitation pulses at > 30 dB using a dual feedback system for increased dynamic range. BS: beam splitter; PC: polarization controller; VOA: variable optical attenuator; LP: linear polarizer; SPAD: single-photon avalanche diode. (b), (c) **Time-resolved QD resonance fluorescence under 100-ps π -pulse excitation.** We overlay pulsed RF on a real-time measurement of the 100-ps excitation pulse (with spectral FWHM $\sim 5.4 \mu\text{eV}$, see Supplemental Document) obtained by tapping off some of the power from the EOM output [see (a)]. A fit of a single exponential function to the exciton decay yields lifetimes of $T_1^{X^{1-}} = 0.79(1)$ ns and $T_1^{X^0} = 0.78(2)$ ns for X^{1-} and X^0 respectively. The V-type energy structure of X^0 leads to quantum beats between excited states which are directly detected here in the pulsed RF transient decay. (d) **Direct observation of Rabi oscillations in the charged exciton.** A fit of the theoretical excited state population (see Supplemental Document) to the Rabi oscillations gives a dephasing time $T_2 = (2.1 \pm 0.2)T_1$.

tical pulses have been used for direct detection of Rabi oscillations in QD excitons ($w = 2$ ns) [4], as well as fast triggering of single-photon generation with a large multi-photon contribution in the emission due to large trigger pulse widths ($w > 300$ ps) [22]. EOMs have also been applied for triggered photon generation from a QD also using optical pulses with $w \geq 400$ ps specifically applied to QD spin manipulation and quantum teleportation [23].

Efforts have also been made to synchronously modulate QD photoluminescence generated using pulsed optical pumping with the goal of waveform shaping and temporal matching [24], as well as improved single-photon generation by filtering out multi-photon events and the incoherent portion of the photon wave packets [25]. The uses of EOMs for modulation of single-photon wave packets generated in pulsed mode by non-QD sources have also been demonstrated [26, 27].

In all these works, on-demand operation and pure single-photon generation of the sources have been under-

mined by high background counts and the widths of the excitation pulses. We use an EOM to demonstrate narrower optical-excitation-pulse widths and low background counts in the on-demand single-photon emission from a QD, better highlighting the potential of the flexible triggering for high-quality indistinguishable single-photon generation. We also exploit the flexibility of our setup for a detailed experimental study of the effect of finite duration of excitation π pulses on the degree of photon antibunching.

II. METHODS

A. Sample details. Our experiments were performed on self-assembled InGaAs quantum dots embedded in a GaAs Schottky diode for deterministic charge-state control. A broadband planar cavity antenna is used to enhance the photon extraction efficiency [28]. The QDs are

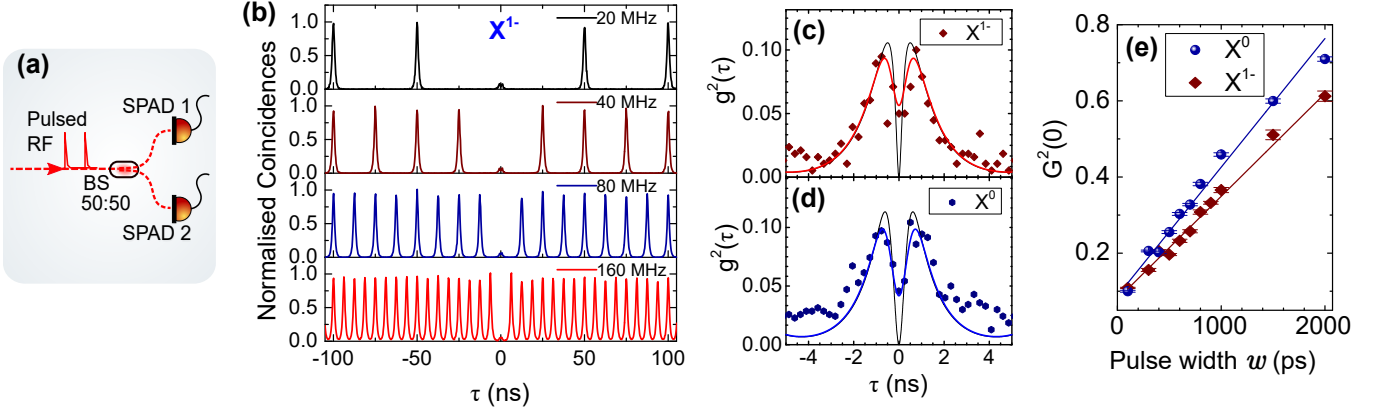


FIG. 2. **Pulsed antibunching of on-demand triggered resonance-fluorescence photons.** (a) Measurement setup (b) Demonstration of flexible triggering of single-photon generation with examples at various frequencies. All measurements have a 180-s integration time. (c) and (d) show zooms into the time-zero peaks revealing ideal antibunching smeared out by jitter in our detection system (FWHM ~ 150 ps). The data points represent raw experimental data, while the solid coloured ($g^2(0) \simeq 0.05$) and black ($g^2(0) = 0.0$) lines respectively represent the results of quantum numerical simulation of the master equation (see Section SII of the Supplemental Document for details) with and without convolution with the instrument response function (IRF) of our detection system (FWHM ~ 150 ps). The pulsed antibunching is limited by the effect of the finite width of our excitation 100-ps pulses (the limit of our pulse generator) giving $G_{\text{exp}}^2(0) \simeq 0.1$ and $g_{\text{exp}}^2(0) \simeq 0.05$. (e) $G^2(0)$ as a function excitation pulse width under π -pulse excitation. Measurements were performed on both neutral and charged exciton states. The solid lines are linear fits to the experimental data.

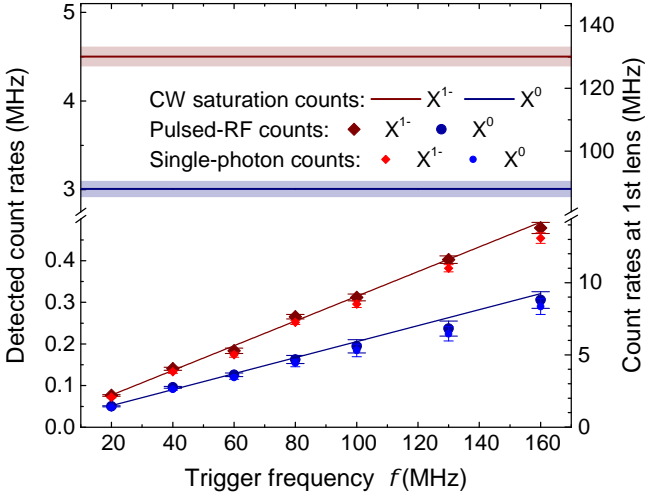


FIG. 3. **Count rates as a function of trigger pulse frequency.** Raw experimental count rates on the detector are plotted for both X^0 and X^{1-} , as well as single photon count rates which are calculated from corresponding multiphoton probabilities [$G^2(0)$]. CW saturation counts are also shown for comparison.

at an antinode of a fifth-order planar cavity on top of a Au layer which functions simultaneously as a cavity mirror and Schottky gate. Simulations predict a photon extraction efficiency of $\sim 27\%$ into the first objective lens from this device.

B. Resonance fluorescence system. We perform

pulsed RF measurements on both the neutral exciton (X^0) and charged exciton states (X^{1-}) of a quantum dot. Our setup for triggering single-photon generation on demand is illustrated in Fig. 1(a). For RF, we use a cross-polarization technique in which orthogonally oriented linear polarizers are placed in the excitation and collection arms of a confocal microscope to suppress resonant-excitation-laser photons in the collected light [20], with extinction ratios of more than 10^7 in CW operation.

C. Pulsed trigger generation. We generate our optical excitation trigger signals using a programmable pulse-pattern generator (PPG) which produces electronic pulses with widths of down to $w = 100$ ps at up to 3.35 GHz (period $T \simeq 300$ ps). Notably, much faster pulses ($w < 30$ ps) can be achieved in the future with commercially available electronic pulse generators. The PPG drives a 20-Gb/s EOM which in turn modulates the output of a resonant CW laser to obtain optical pulses practically identical to the driving electronic pulses with typical extinction ratios in excess of 30 dB. This extinction ratio is actively maintained by a modulator bias controller (MBC) optoelectronic circuit through optical feedback. We are able to vary pulse widths and repetition rates of the trigger pulses with high precision, and also obtain optical pulses with user-defined bit-cycle data patterns.

D. Efficiencies. The efficiency of our microscope and detectors are as follows: coupling of far-field radiation into single-mode fiber: $\sim 31.4\%$; linear polarizer: 43%; beam splitter surfaces: $(96\%)^4$; SPAD at $\lambda \sim 950$ nm: $\sim 30\%$. The combination gives $\sim 3.5\%$. The combination gives $\sim 3.5\%$. The measured total efficiency of detecting a single photon per trigger pulse is $\sim 0.36\%$. Based on

this, we determine the photon extraction efficiency from the sample into the first lens to be $\sim 10.4\%$.

III. RESULTS

Fig. 1(a) illustrates our basic excitation and measurement setup. In Fig. 1(b) and (c), we respectively show time-resolved RF from the charged exciton state X^{1-} and X^0 following excitation with a π pulse ($w = 100$ ps), which gives exciton lifetimes of $T_1^{X^{1-}} = 0.79 \pm 0.01$ ns and $T_1^{X^0} = 0.78 \pm 0.02$ ns. The V-type energy structure of X^0 leads to quantum beats between excited states (e.g., see [29]) which are directly detected here in the pulsed RF transient decay. The beat frequency corresponds to the fine-structure splitting (due to electron-hole exchange interaction) of $\delta_0 = 3.3$ GHz for this QD. In Fig. 1(d), we demonstrate direct measurement of X^{1-} Rabi oscillations using 2-ns pulses from which we extract a dephasing time of $T_2 = 1.66 \pm 0.18$ ns, using the lifetime of $T_1 = 0.79 \pm 0.01$ ns obtained from the measured X^{1-} decay with 100-ps pulses. This is consistent with the case of no pure dephasing where $T_2 = 2T_1$, confirming the absence of excitation induced dephasing effects [30, 31]. The first peak in the RF counts corresponds to a pulse area of π . We confirm the π -pulse area/power both using the direct measurement and by conventional methods (e.g., as used in Ref. [10]).

Antibunching and efficiency. For our main autocorrelation measurements, we excite the quantum dot with 100-ps π pulses. Fig. 2(a) shows a schematic of the Hanbury Brown and Twiss (HBT)-type set-up used in our antibunching measurements. In what follows, while we will use $g^2(\tau)$ to represent the autocorrelation function of the continuous time delay τ , $G^2(\tau_n)$ denotes the pulsed-mode autocorrelation function of the discretised time delay $\tau_n = nT$ obtained by integrating the n^{th} pulse in $g^2(\tau)$, where $T = 1/f$ is the pulse period. In Fig. 2(b), we demonstrate antibunching at various trigger frequencies as seen in the intensity-correlation histograms for the RF emission from the QD under pulsed excitation. Pulsed second-order correlation at zero delay $G^2(0)$ are calculated by integrating photon counts in the zero-time-delay peak and dividing by the average of the adjacent peaks over a range of ~ 650 ns around the time-zero peak, with standard deviations obtained from propagated Poissonian counting statistics of the raw counts. With 100-ps π pulses, we obtain raw experimental values $G^2(0) \sim 0.1$, and $g^2(0) \sim 0.05$, as shown in Figs 2 (c-e). An increase in pulse widths leads to worse pulsed antibunching $G^2(0)$ [Fig. 2(e)], while $g^2(0)$ values are unaffected.

We demonstrate the flexibility of the system and how it may be exploited to, e.g., maximize single-photon rates by performing autocorrelation measurements at varying repetition rates of 20 MHz to 160 MHz and detect up to ~ 0.45 MHz of single photon counts (see Fig. 3). Also shown are the detected counts rates at saturation in CW mode for each charge state. Peak coincidence counts of

up to 5.5 K are measured at 160 MHz with a 256-ps time bin size in 180-s acquisitions. Beyond ~ 160 MHz, the pulses in the RF autocorrelation function begin to overlap. This limit is imposed by the exciton lifetime. Single-photon count rates are obtained using the emission probability of more than one photon in a pulse, as obtained from the corresponding values of $G^2(0)$. From the count rates, we calculate the overall efficiency, i.e. probability to detect a pure single photon state per trigger π -pulse to be $0.36 \pm 0.01\%$. Based on the combined efficiency of the collection optics and detectors ($\sim 3.5\%$, see Methods), we determine an extraction efficiency of $10.4 \pm 0.7\%$ into the first lens while the simulated extraction efficiency for our sample is $\sim 27\%$ for a 0.68-NA objective lens (as used in our experiment) [28].

To reveal the nature of the non-ideal raw antibunching measured in our pulsed experiments and verify the true quality of our single-photon source, we perform high timing resolution (jitter ~ 150 ps) measurements of the intensity autocorrelation. Figs 2 (c) and (d) show zooms into the small time-zero peaks for X^{1-} and X^0 , which both reveal characteristic central dips. At zero delay, we see clear antibunching within the small peak with a vanishing raw multiphoton probability of $g^2(0) = 0.05$. To provide further insight, we use numerical simulations of the master equation for both X^0 and X^{1-} (at a magnetic field of $B_{\text{ext}} = 0$), as a V-type atomic system and a two-level system, respectively (see Section SII of the Supplemental Document for details). The small peaks surrounding $\tau = 0$ also manifest in the simulation results, in good agreement with the experimental data as shown in Figs 2 (c) and (d). The underlying mechanism of this non-ideality is a small probability to re-excite the system (following a first photon emission event) within the pulse duration. The re-excitation probability increases with pulse width, as confirmed in the simulation and experimentally [see Fig. 2(e)]. Importantly, the $g^2(0)$ is always zero at the middle of the time-zero peak, indicating that arbitrarily low $g^2(0)$ values can be achieved with shorter excitation pulses. Taking the IRF of our detection system into account, we estimate perfect antibunching ($g^2(0) = 0.0$). We conclude that, although more than one photon may be emitted during the 100-ps-long excitation pulse with a small probability, these photons are not emitted at the same time.

Pulsed two-photon interference. For TPI measurements, we send the QD photons into a HOM-type setup [see Fig. 4(a)] which consists of an unbalanced Mach-Zender (MZ) interferometer with delay of $\Delta t = 49.70$ ns and polarization control in each arm to enable measurements with parallel (\parallel) and orthogonal (\perp) polarizations of interfering photons. The beamsplitters in the MZ setup have nearly perfect 50:50 splitting ratios. We filter out the zero-phonon line from the most of the phonon sideband using a grating-based spectral filter (bandwidth $\Delta f = 12$ GHz and efficiency $\eta_f = 22\%$). Due to the flexibility of trigger pulse generation, we are able to precisely match the repetition period of the pulses to

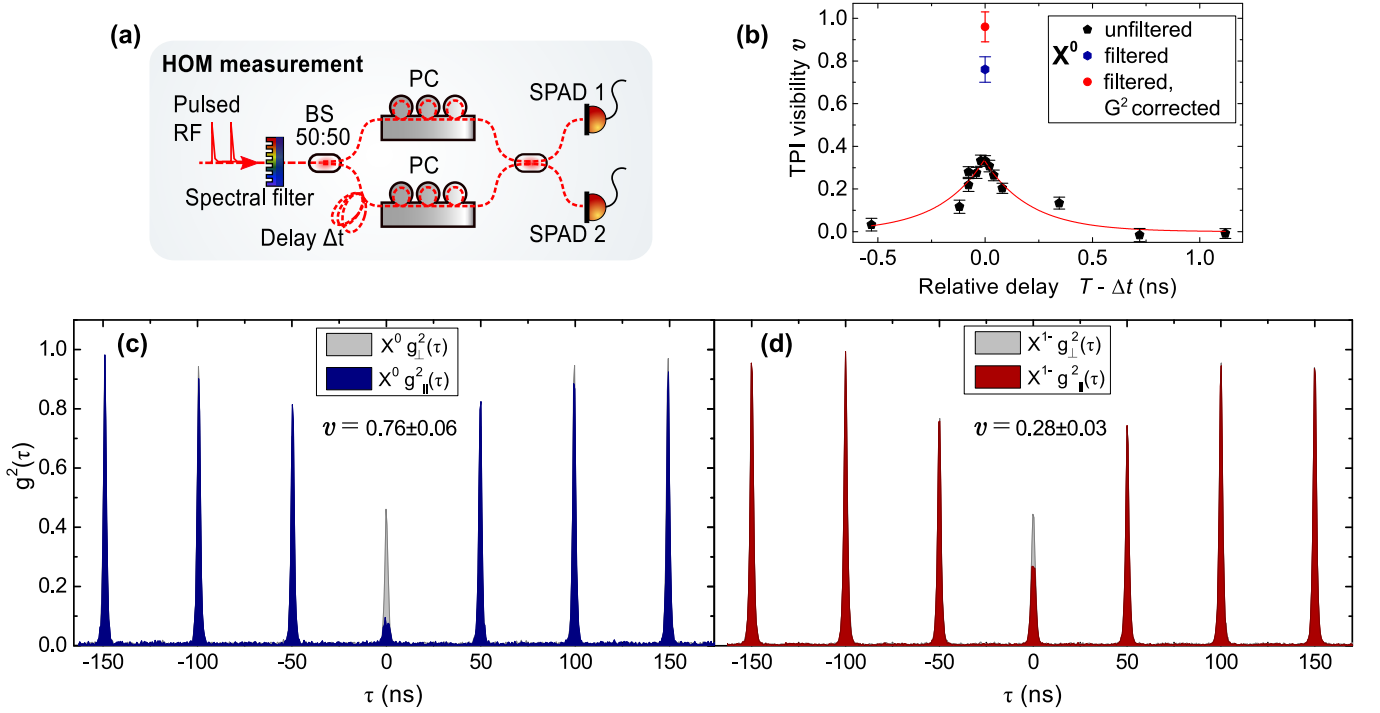


FIG. 4. **Demonstration of indistinguishability of single photons triggered on demand.** (a) Hong-Ou-Mandel (HOM)-type two-photon interference (TPI) results. The flexibility of our approach allows us to set the pulse period to match the delay in our HOM setup ($\Delta t = 49.7$ ns). (b) **TPI visibility versus period.** The measurements were performed on a neutral exciton line for X^0 using various pulse periods and hence delays between interfering photons with π -pulse excitation. **TPI autocorrelation at zero relative delay.** (c) shows results for X^0 photons and (d) for the charged exciton (X^{1-}) both at $B_{\text{ext}} = 0$ T. Measurements were performed using 100-ps-wide excitation pulses. The measurements plotted in grey are with orthogonal polarizations of interfering photons. (c) and (d) are measured with most of the phonon band filtered out using a grating-based spectral filter. The X^0 photons show TPI visibilities of $v = 0.76 \pm 0.06$ as raw experimental data and $v = 0.96 \pm 0.07$ when corrected *only* for multiphoton emission (G^2 corrected).

Δt (see Fig. 4(b)) to obtain pulsed autocorrelation at a relative delay $T - \Delta t = 0$, shown in Figs 4(c) and (d). The TPI visibility is defined as $v = [G^2_{\perp}(0) - G^2_{\parallel}(0)]/G^2_{\perp}(0)$. For the X^0 and X^{1-} , we measure raw visibilities of $v = 0.76 \pm 0.06$ and 0.28 ± 0.03 respectively. The raw indistinguishability of the X^0 photons is limited primarily by the multiphoton probability of $G^2(0) = 0.10 \pm 0.01$, which is in turn limited by the excitation pulse width as described above. When this is corrected for (by using $G'^2_{\parallel}(0) = G^2_{\parallel}(0) - G^2(0)$), we obtain a TPI visibilities of $v = 0.96 \pm 0.06$ and 0.47 ± 0.03 respectively for X^0 and X^{1-} without accounting for any other experimental imperfections. The reduced visibility of the X^{1-} ($B_{\text{ext}} = 0$ T) is understood to be due to detuned Raman-scattered photons which are distinguishable from both the elastic and incoherent components of the resonance fluorescence due to nuclear spin fluctuations (further details are provided in Ref. [32]). We stress that the Raman-scattered photons result in a total linewidth of less than 1 GHz which is not filtered out by the 12-GHz-bandwidth spectral filter.

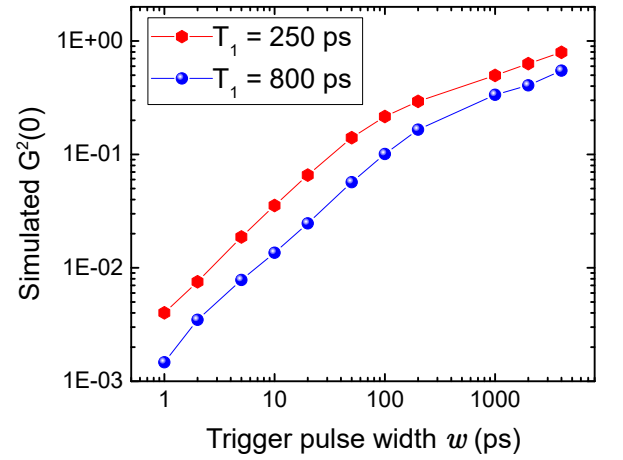


FIG. 5. **Simulated $G^2(0)$ as a function of excitation pulse width under 0.81π -pulse excitation.** Simulation of a two-level system with lifetimes $T_1 = 800$ ps and 250 ps using a Gaussian (temporal) 0.81π -excitation pulse profiles with varying widths. We use 0.81π for the simulated Gaussian pulses because with a 100-ps width, they give the same $G^2(0)$ as the asymmetric 100-ps π pulses used in the experiment.

IV. DISCUSSION

For on-demand single photon sources to underpin scalable and efficient linear-optical quantum computing and networking, stringent criteria must be satisfied [33, 34]. Our experimental results provide insight into the prospect of realizing the $G^2(0)$ requirements using resonance-fluorescence-generated single photons. A crucial result is the effect of the pulse width relative to T_1 on $G^2(0)$. Typically, Purcell enhancement is considered desirable to reduce the impact of dephasing mechanisms [35–37] and enable increased clock rates. However, in pulsed RF a faster T_1 also increases the probability for re-excitation given a certain excitation pulse width. We illustrate this trade-off using a numerical simulation for $G^2(0)$ as a function of pulse width (Gaussian profile) for $T_1 = 250\text{ps}$ and 800ps (Fig. 5). We see that in both cases vanishing $G^2(0)$ can be obtained for ultra-short pulse widths, but practically the minimization of $G^2(0)$ is best achieved with larger T_1 values. This is important for prospective applications (such as linear-optical QIP) of single photons generated using pulsed resonance fluorescence.

We have demonstrated flexible electronic triggering of on-demand single indistinguishable photons. This system offers several intriguing advantages for future applications. Whereas ultra-short excitation pulses lead to excitation induced dephasing (EID) [31], coherent control with longer pulse durations is expected to minimize EID [38, 39]. Hence, for some coherent control and read-out schemes the flexibility of electronically tunable pulse

durations is likely to be attractive. Another advantage of this approach is the possibility to specifically tailor the pump pulses for quantum control processes such as stimulated Raman adiabatic passage [40] in quantum dots exhibiting spin-Lambda systems [41, 42]. Finally, we note that the flexible technique presented here enables an excitation repetition rate up to the limit of that imposed by T_1 , offering a significant boost in count rates for real applications. While overall system efficiencies need to be improved to realize an ideal single-photon source, recent developments in QIP protocols have made efficiency requirements considerably less stringent (e.g., in [33] efficient linear optical quantum computation is possible with an overall efficiency of $2/3$) even as high quality indistinguishability, antibunching, and brightness are now simultaneously being achieved (e.g., see [13–15]). The approach we demonstrate here is an important step towards combining these key performance features with true on-demand operation.

Funding and Acknowledgements. The authors would like acknowledge the financial support for this work from the Engineering and Physical Sciences Research Council (EPSRC) (EP/G03673X/1, EP/I023186/1, EP/K015338/1) and the European Research Council (ERC) (307392). B.D.G acknowledges the Royal Society for support via a University Research Fellowship. The KIST authors acknowledge support from KIST’s flagship program and GRL.

-
- [1] H. J. Kimble, “The quantum internet,” *Nature* **453**, 1023–1030 (2008).
 - [2] P. Kok, W. J. Munro, K. Nemoto, T. C. Ralph, J. P. Dowling, and G. J. Milburn, “Linear optical quantum computing with photonic qubits,” *Reviews of Modern Physics* **79**, 135–174 (2007).
 - [3] J. L. O’Brien, A. Furusawa, and J. Vučković, “Photonic quantum technologies,” *Nature Photonics* **3**, 687–695 (2009).
 - [4] P. P. Rohde and T. C. Ralph, “Error tolerance of the boson-sampling model for linear optics quantum computing,” *Physical Review A* **85**, 022332 (2012).
 - [5] H. J. Briegel, W. Dur, J. I. Cirac, and P. Zoller, “Quantum Repeaters: The Role of Imperfect Local Operations in Quantum Communication,” *Physical Review Letters* **81**, 5932–5935 (1998).
 - [6] J. B. Spring, B. J. Metcalf, P. C. Humphreys, W. S. Kolthammer, X.-M. Jin, M. Barbieri, A. Datta, N. Thomas-Peter, N. K. Langford, D. Kundys, J. C. Gates, B. J. Smith, P. G. R. Smith, and I. A. Walmsley, “Boson Sampling on a Photonic Chip,” *Science* **339**, 798–801 (2013).
 - [7] M. A. Broome, A. Fedrizzi, S. Rahimi-Keshari, J. Dove, S. Aaronson, T. C. Ralph, and A. G. White, “Photonic Boson Sampling in a Tunable Circuit,” *Science* **339**, 794–798 (2013).
 - [8] B. Lounis and M. Orrit, “Single-photon sources,” *Reports on Progress in Physics* **68**, 1129 (2005).
 - [9] A. J. Shields, “Semiconductor quantum light sources,” *Nature Photonics* **1**, 215–223 (2007).
 - [10] Y.-M. He, Y. He, Y.-J. Wei, D. Wu, M. Atatüre, C. Schneider, S. Höfling, M. Kamp, C.-Y. Lu, and J.-W. Pan, “On-demand semiconductor single-photon source with near-unity indistinguishability,” *Nature Nanotechnology* **8**, 213–217 (2013).
 - [11] M. Müller, S. Bounouar, K. D. Jöns, M. Glässl, and P. Michler, “On-demand generation of indistinguishable polarization-entangled photon pairs,” *Nature Photonics* **8**, 224–228 (2014).
 - [12] T. Huber, D. Föger, G. Solomon, and G. Weihs, “Optimal excitation conditions for indistinguishable photons from quantum dots,” *arXiv:1507.07404* (2015).
 - [13] X. Ding, Y. He, Z. C. Duan, N. Gregersen, M. C. Chen, S. Unsleber, S. Maier, C. Schneider, M. Kamp, S. Höfling, C.-Y. Lu, and J.-W. Pan, “On-Demand Single Photons with High Extraction Efficiency and Near-Unity Indistinguishability from a Resonantly Driven Quantum Dot in a Micropillar,” *Physical Review Letters* **116**, 020401 (2016).
 - [14] J. C. Lored, N. A. Zakaria, N. Somaschi, C. Anton, L. D. Santis, V. Giesz, T. Grange, M. A. Broome, O. Gaz-

- zono, G. Coppola, I. Sagnes, A. Lemaître, A. Auffèves, P. Senellart, M. P. Almeida, and A. G. White, “Scalable performance in solid-state single-photon sources,” arXiv:1601.00654 (2016).
- [15] N. Somaschi, V. Giesz, L. De Santis, J. C. Lored, M. P. Almeida, G. Hornecker, S. L. Portalupi, T. Grange, C. Anton, J. Demory, C. Gomez, I. Sagnes, N. D. Lanzillotti-Kimura, A. Lemaître, A. Auffèves, A. G. White, L. Lanco, and P. Senellart, “Near-optimal single-photon sources in the solid state,” *Nature Photonics Advance Online Publication* doi:10.1038/nphoton.2016.23 (2016).
- [16] C. K. Hong, Z. Y. Ou, and L. Mandel, “Measurement of subpicosecond time intervals between two photons by interference,” *Physical Review Letters* **59**, 2044–2046 (1987).
- [17] J. H. Prechtel, P. A. Dalgarno, R. H. Hadfield, J. McFarlane, A. Badolato, P. M. Petroff, and R. J. Warburton, “Fast electro-optics of a single self-assembled quantum dot in a charge-tunable device,” *Journal of Applied Physics* **111**, 043112 (2012).
- [18] Y. Cao, A. J. Bennett, D. J. P. Ellis, I. Farrer, D. A. Ritchie, and A. J. Shields, “Ultrafast electrical control of a resonantly driven single photon source,” *Applied Physics Letters* **105**, 051112 (2014).
- [19] A. Schlehahn, M. Gaafar, M. Vaupe, M. Gschrey, P. Schnauber, J. H. Schulze, S. Rodt, A. Strittmatter, W. Stolz, A. Rahimi-Iman, T. Heindel, M. Koch, and S. Reitzenstein, “Single-photon emission at a rate of 143 MHz from a deterministic quantum-dot microlens triggered by a mode-locked vertical-external-cavity surface-emitting laser,” *Applied Physics Letters* **107**, 041105 (2015).
- [20] C. Matthiesen, M. Geller, C. H. H. Schulte, C. Le Gall, J. Hansom, Z. Li, M. Hugues, E. Clarke, and M. Atature, “Phase-locked indistinguishable photons with synthesized waveforms from a solid-state source,” *Nature Communications* **4**, 1600 (2013).
- [21] J. R. Schaibley, A. P. Burgers, G. A. McCracken, D. G. Steel, A. S. Bracker, D. Gammon, and L. J. Sham, “Direct detection of time-resolved Rabi oscillations in a single quantum dot via resonance fluorescence,” *Physical Review B* **87**, 115311–5 (2013).
- [22] K. Rivoire, S. Buckley, A. Majumdar, H. Kim, P. Petroff, and J. Vučković, “Fast quantum dot single photon source triggered at telecommunications wavelength,” *Applied Physics Letters* **98**, 083105 (2011).
- [23] W. Gao, P. Fallahi, E. Togan, A. Delteil, Y. Chin, J. Miguel-Sanchez, and A. Imamoglu, “Quantum teleportation from a propagating photon to a solid-state spin qubit,” *Nature Communications* **4**, 2744 (2013).
- [24] M. T. Rakher and K. Srinivasan, “Subnanosecond electro-optic modulation of triggered single photons from a quantum dot,” *Applied Physics Letters* **98**, 211103 (2011).
- [25] S. Ates, I. Agha, A. Gulnatti, I. Rech, A. Badolato, and K. Srinivasan, “Improving the performance of bright quantum dot single photon sources using temporal filtering via amplitude modulation,” *Scientific Reports* **3**, 1397 (2013).
- [26] P. Kolchin, C. Belthangady, S. Du, G. Yin, and S. Harris, “Electro-optic modulation of single photons,” *Physical Review Letters* **101**, 103601 (2008).
- [27] H. P. Specht, J. Bochmann, M. Mücke, B. Weber, E. Figueroa, D. L. Moehring, and G. Rempe, “Phase shaping of single-photon wave packets,” *Nature Photonics* **3**, 469–472 (2009).
- [28] Y. Ma, P. E. Kremer, and B. D. Gerardot, “Efficient photon extraction from a quantum dot in a broad-band planar cavity antenna,” *Journal of Applied Physics* **115**, 023106 (2014).
- [29] T. Flissikowski, A. Hundt, M. Lowisch, M. Rabe, and F. Henneberger, “Photon Beats from a Single Semiconductor Quantum Dot,” *Physical Review Letters* **86**, 3172–3175 (2001).
- [30] E. S. Kyoseva and N. V. Vitanov, “Resonant excitation amidst dephasing: An exact analytic solution,” *Physical Review A* **71**, 054102 (2005).
- [31] A. J. Ramsay, A. V. Gopal, E. M. Gauger, A. Nazir, B. W. Lovett, A. M. Fox, and M. S. Skolnick, “Damping of Exciton Rabi Rotations by Acoustic Phonons in Optically Excited InGaAs/GaAs Quantum Dots,” *Physical Review Letters* **104**, 017402 (2010).
- [32] R. N. E. Malein, T. S. Santana, J. M. Zajac, A. C. Dada, E. M. Gauger, P. M. Petroff, J. Y. Lim, J. D. Song, and B. D. Gerardot, “Screening nuclear field fluctuations in quantum dots for indistinguishable photon generation,” arXiv:1509.01057v1 (2015).
- [33] M. Varnava, D. E. Browne, and T. Rudolph, “How Good Must Single Photon Sources and Detectors Be for Efficient Linear Optical Quantum Computation?” *Physical Review Letters* **100**, 060502 (2008).
- [34] T. Jennewein, M. Barbieri, and A. G. White, “Single-photon device requirements for operating linear optics quantum computing outside the post-selection basis,” *Journal of Modern Optics* **58**, 276–287 (2011).
- [35] C. Santori, D. Fattal, J. Vučković, G. S. Solomon, and Y. Yamamoto, “Indistinguishable photons from a single-photon device,” *Nature* **419**, 594–597 (2002).
- [36] S. Laurent, S. Varoutsis, L. Le Gratiet, A. Lemaître, I. Sagnes, F. Raineri, A. Levenson, I. Robert-Philip, and I. Abram, “Indistinguishable single photons from a single-quantum dot in a two-dimensional photonic crystal cavity,” *Applied Physics Letters* **87**, 163107 (2005).
- [37] O. Gazzano, S. Michaelis de Vasconcellos, C. Arnold, A. Nowak, E. Galopin, I. Sagnes, L. Lanco, A. Lemaître, and P. Senellart, “Bright solid-state sources of indistinguishable single photons,” *Nature Communications* **4**, 1425 (2013).
- [38] J. Förstner, C. Weber, J. Danckwerts, and A. Knorr, “Phonon-Assisted Damping of Rabi Oscillations in Semiconductor Quantum Dots,” *Physical Review Letters* **91**, 127401 (2003).
- [39] P. Machnikowski and L. Jacak, “Resonant nature of phonon-induced damping of Rabi oscillations in quantum dots,” *Physical Review B* **69**, 193302 (2004).
- [40] K. Bergmann, H. Theuer, and B. W. Shore, “Coherent population transfer among quantum states of atoms and molecules,” *Rev. Mod. Phys.* **70**, 1003–1025 (1998).
- [41] X. Xu, Y. Wu, B. Sun, Q. Huang, J. Cheng, D. G. Steel, A. S. Bracker, D. Gammon, C. Emary, and L. J. Sham, “Fast spin state initialization in a singly charged InGaAs quantum dot by optical cooling,” *Phys. Rev. Lett.* **99**, 097401 (2007).
- [42] D. Brunner, B. D. Gerardot, P. A. Dalgarno, G. Wüst, K. Karrai, N. G. Stoltz, P. M. Petroff, and R. J. Warburton, “A coherent single-hole spin in a semiconductor,” *Science* **325**, 70–72 (2009).

Supplementary Information for: “Indistinguishable single photons with flexible electronic triggering”

SI. NUMERICAL SIMULATION FOR PULSED RESONANCE FLUORESCENCE

Our numerical simulation is based on the master equation method (e.g., see [1–3]). We use the well known Hamiltonians describing a driven (1) two-level atom for the X^{1-} and (2) V-type three level atom for X^0 state of the InGaAs quantum dot (see Fig. S1).

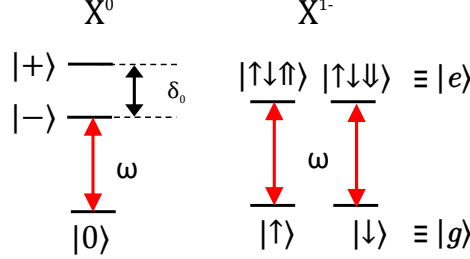


FIG. S1. **Level diagrams for X^0 and X^{1-} at an external magnetic field of $B_{ext} = 0$.** The X^{1-} is modelled as a two-level system (due to the degeneracy of the excited and ground state levels), and the X^0 as a V-type three-level system. δ_0 is the electron-hole exchange interaction energy, the red arrows represent the driving field and ω its frequency.

The Hamiltonian for the two-level system is

$$\hat{H}_{X^{1-}} = \frac{\Delta}{2}(|e\rangle\langle e| - |g\rangle\langle g|) + \frac{\Omega}{2}(|g\rangle\langle e| + |e\rangle\langle g|), \quad (S1)$$

while for X^0 , we have

$$\begin{aligned} \hat{H}_{X^0} = & \frac{\Delta}{2}(|-\rangle\langle -| - |0\rangle\langle 0|) + \left(\frac{\Delta}{2} + \delta_0\right)|+\rangle\langle +| + \\ & \frac{\Omega}{2}[\cos\theta(|-\rangle\langle 0| + |0\rangle\langle -|) + \sin\theta(|+\rangle\langle 0| + |0\rangle\langle +|)], \end{aligned} \quad (S2)$$

under the rotating-wave approximation. Δ is the detuning between the driving field and the transition from $|0\rangle$ ($|g\rangle$) to $|-\rangle$ ($|e\rangle$), δ_0 the electron-hole interaction energy (corresponding to a fine-structure splitting of $13\mu\text{eV}$ for the QD reported in Figs 1-4 of the manuscript). Ω represents the Rabi frequency, θ is a constant determined by the polarization angle of the (linearly polarized) driving field.

Spontaneous decay and dephasing are included in the time evolution of the system via the Lindblad terms of the master equation. The Lindblad operator acting on the density matrix ρ (for a given collapse operator \hat{C}) is defined as

$$L(\hat{C})\rho = \hat{C}\rho\hat{C}^\dagger - \frac{1}{2}(\hat{C}^\dagger\hat{C}\rho + \rho\hat{C}^\dagger\hat{C}) \quad (S3)$$

The master equation can then be written as

$$\dot{\rho} = -\frac{i}{\hbar}[\rho, \hat{H}] + \sum_{ij} \Gamma_{ij} L(\sigma_{ij})\rho. \quad (S4)$$

Here, $\sigma_{ij} = |i\rangle\langle j|$, Γ_{ij} is the decay rate from state $|j\rangle$ to $|i\rangle$ and Γ_{ii} represents the pure dephasing rate of state $|i\rangle$, where $i, j = e, g, 0, +, -$. For example, $\Gamma_{eg} = 1/T_1$, $\Gamma_{ee} = \Gamma_{gg} = 1/T_2 - 1/2T_1 = 0$ for $T_2 = 2T_1$ where T_1 is the exciton lifetime, and $1/T_2$ is the total dephasing rate.

Using the Runge-Kutta fourth-order method, we obtain numerical solutions of the master equation and calculate the autocorrelation function from the obtained density matrix elements. We simulate pulsed excitation by incorporating the corresponding temporal pulse intensity profile and pattern into the driving field $\Omega(t)$ as $I(t) \propto \Omega(t)^2$.

While we use Gaussian temporal pulse profiles to obtain the simulation results in the trend shown in Fig. 5 of the primary manuscript, for the results shown in Fig. 2(c) and (d), we use a ~ 100 -ps-wide lognormal temporal profile which is obtained by fitting to the intensity profile measured from the EOM output. This closely matches the (asymmetric) intensity profile of our excitation pulses.

SII. MODULATION SETUP

We use a z-cut electro-optic modulator having a dual bias-port (for coarse- and fine-tuning) with $V_\pi = 2\text{V}$ to cause the phase shift required to change from minimum to maximum transmission. The EOM is driven by a PPG with a 12.5 Gb/s pulse amplifier at the output to ensure full modulation depth. As mentioned in the main manuscript, the high modulation extinction ratio is achieved and actively maintained by a modulator bias controller which uses two photodetectors, with different sensitivities. The lower(higher)-sensitivity detector is used in the coarse(fine) tuning of the modulator bias. Two 95:5 beam splitters are used to tap off light from the EOM output for coupling to the respective photo-detectors.

SIII. SPECTRAL PROFILE OF EXCITATION PULSES

We characterise the spectral profile of the 100-ps pulses from the output of the electro-optic modulator (EOM) used in the experiment with a Fabry-Perot scanning interferometer having 27-MHz resolution and a free spectral range of 5.5 GHz. There is a broadening of the modulated light in the spectral domain as compared with the continuous-wave (CW) light, with longer pulses exhibiting narrower spectral widths as expected. Fig. S2 compares the measured frequency-domain profile of the 100-ps pulses used for the two-photon interference and antibunching measurements reported in the manuscript with those of 1-ns and 4-ns pulses.

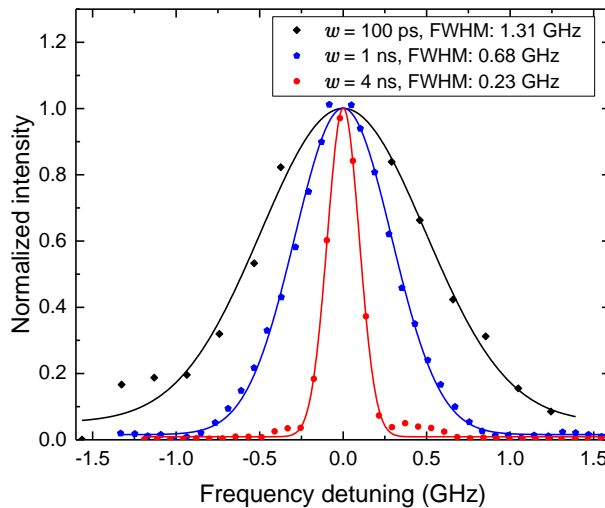


FIG. S2. **High resolution spectrum of excitation pulses at different pulse widths w .** The points and lines respectively represent experimental data and fits of Gaussian functions to the data, from which we obtain a full-width-at-half-maximum (FWHM) of $1.3 \pm 0.1\text{ GHz}$ ($5.4 \pm 0.4\mu\text{eV}$) for the 100-ps pulses.

SIV. RF SPECTRUM/FILTERING IN TPI MEASUREMENTS

As mentioned in the main manuscript, the RF photons were spectrally filtered using a 12-GHz-bandwidth grating-based filter for the TPI experiment. We show typical spectral data for a 100-ps pulsed RF from a quantum dot in our sample in Fig. S3 to compare the unfiltered RF spectral widths with the filter bandwidth. We show the pulsed RF spectrum on a Log scale to highlight the phonon sideband. In this QD the phonon sideband to zero-phonon line ratio is $\sim 1 : 9$.

SV. FITTING FUNCTION FOR RABI-OSCILLATIONS MEASUREMENT

The function fitted to the Rabi oscillation data describing the probability of being in the excited state is obtained by solving the density-matrix equations for a resonant driving field, including the effects of decoherence due to

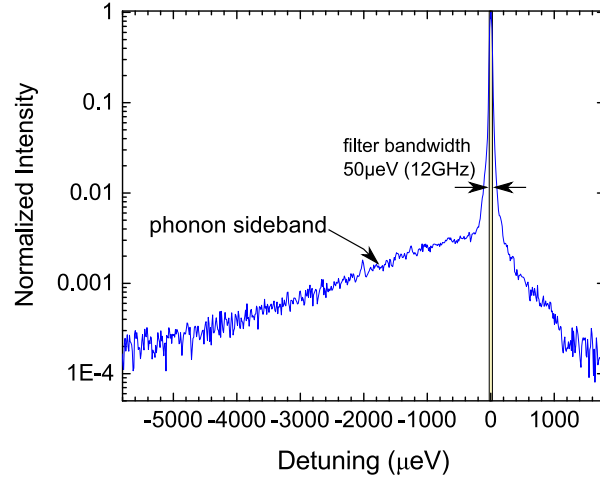


FIG. S3. **High-power spectrum of RF photons under 100-ps pulsed excitation**. Typical spectral data for a 100-ps pulsed RF from a single quantum dot ($\lambda \sim 960\text{nm}$) in our sample with no filtering plotted on log scale to show the phonon sideband and showing the bandwidth of the filter used in the Hong-Ou-Mandel-type TPI measurements. This spectral data was acquired using a $35\text{-}\mu\text{eV}$ resolution grating spectrometer. The linewidth of the zero-phonon line shown here is limited by spectrometer resolution. We note that $> 87\%$ of the total signal spectra lies within the pass band of the filter.

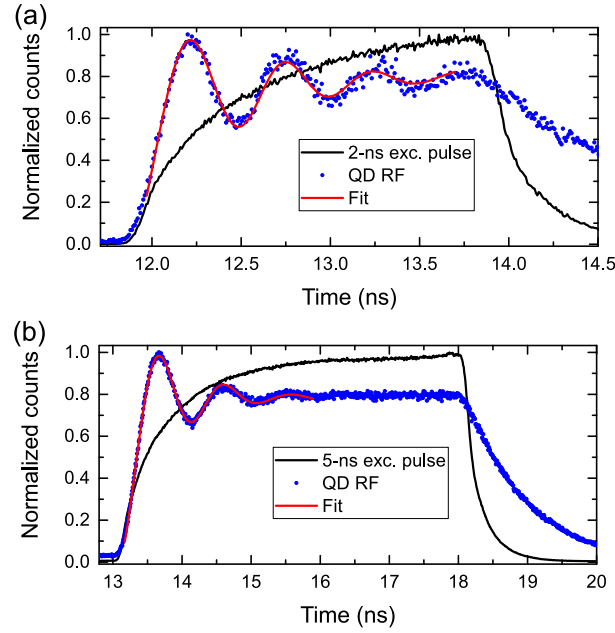


FIG. S4. X^{1-} **Rabi oscillations measurement** using (a) 2-ns at $\sim 188.5\text{ nW}$ peak power and (b) 5-ns excitation pulses at $\sim 55.5\text{ nW}$ peak power. The red line represents a fit of the theoretical excited state population to the Rabi oscillations when the shape of the excitation pulse is taken into account, i.e., using Eq. S7 in Eq. S5 for the fit gives a dephasing time $T_2 = (2.02 \pm 0.27)T_1$.

spontaneous emission and pure dephasing, which is a well known result (e.g., it is the same result used to fit Rabi-oscillation data as reported in Ref. [4]), i.e.,

$$\rho_{22}(t) = \frac{\Omega^2/2}{\Omega^2 + 1/(T_1 T_2)} \times \left\{ 1 - \left[\cos(\xi t) + \frac{1/T_1 + 1/T_2}{2\xi} \sin(\xi t) \right] e^{-\frac{1}{2}(1/T_1 + 1/T_2)t} \right\}. \quad (\text{S5})$$

Here,

$$\xi = \sqrt{\Omega^2 - \frac{(1/T_2 - 1/T_1)^2}{4}}, \quad (\text{S6})$$

Ω is the Rabi frequency, and T_1, T_2 are again the exciton lifetime and the total dephasing time respectively.

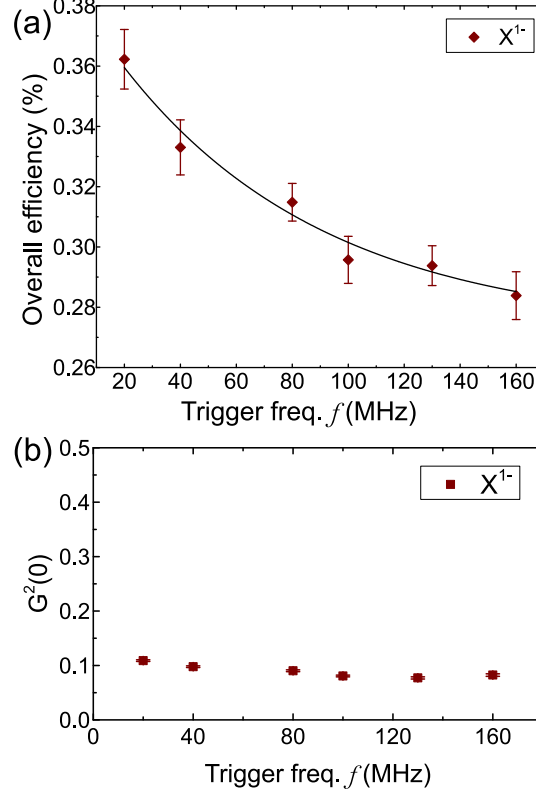


FIG. S5. (a) **Efficiency** and (b) G^2 **trend with varying trigger frequency** under excitation with 100-ps π pulses. An exponential decay was fit to the data in (a). We observe similar values for $G^2(0)$ (≈ 0.1) over the range of trigger frequencies 20 to 160 MHz.

SVI. TEMPORAL PROFILE OF EXCITATION PULSES FOR RABI OSCILLATION MEASUREMENTS

The 2-ns optical excitation pulse which were used for the Rabi oscillation measurement shown in Fig. 1 (d) of the main manuscript is a faithful reproduction of the electrical pulse from the PPG, which has a slow rising edge. The effect of the increasing power over the duration of the 2-ns pulse is to cause a slight chirp (i.e., variation with time) in the frequency of Rabi oscillation Ω . For the result presented in the main manuscript, this effect is not modelled in the function used to fit the Rabi oscillations because it has negligible consequence for the main result of $T_2 = 2T_1$.

Here, we include the effect of the temporal profile of the driving field in the fitting function, by setting Ω not as a constant but as

$$|\Omega(t)|^2 \propto (P_0 + P_1 t + P_2 t^2) \quad (\text{S7})$$

This quadratic function gives an excellent fit to the varying excitation power over the region of the Rabi oscillation fit to the RF from which we obtain the actual parameters P_0 , P_1 and P_2 which we then use to define the time variation of Ω . In Fig. S4, we show examples of fits obtained when we use Eq. S7 in Eq. S5 for the fit. This gives $T_2 = (2.02 \pm 0.27)T_1$ in agreement with the case used to fit the data in the main manuscript in which the excitation

pulse is assumed to be flat. For comparison, we also show the measurement obtained using 5-ns pulses which gives a consistent result.

SVII. EFFICIENCY AND PULSED ANTIBUNCHING AS A FUNCTION OF TRIGGER FREQUENCY

We show plots of $G^2(0)$ and overall efficiency as a function of trigger frequency under excitation with 100-ps π pulses. As shown in Fig. S5(a), we find that the overall efficiency (i.e., the ratio of single-photon count rate and trigger rate) reduces as a function of trigger frequency with π -pulse excitation. We understand this to be mainly due to an artifact caused by the dead time of our TCSPC system which is ≤ 80 ns. In Fig. S5(b), $G^2(0) \sim 0.1$ is fairly constant until $f \sim 160$ MHz. At this point, we observe an onset of a quasi-CW operation caused by overlap between peaks in $g^2(\tau)$ leading to a background of $g^2(\tau)_{min} \sim 0.03$ (see Fig. 2 (b) of the main manuscript). The trigger frequency at which this occurs is determined by the lifetime T_1 .

-
- [1] R. R. Puri, Sections 8.5-7 in *Mathematical methods of quantum optics*, vol. 79 (Springer Science & Business Media, 2001).
 - [2] H.-P. Breuer and F. Petruccione, Sections 3.3-4 in *The theory of open quantum systems* (Oxford university press, 2002).
 - [3] M. Orszag, *Quantum optics: including noise reduction, trapped ions, quantum trajectories, and decoherence* (Springer Science & Business Media, 2007).
 - [4] J. R. Schaibley, A. P. Burgers, G. A. McCracken, D. G. Steel, A. S. Bracker, D. Gammon, and L. J. Sham, “Direct detection of time-resolved Rabi oscillations in a single quantum dot via resonance fluorescence,” *Physical Review B* **87**, 115311–5 (2013).